Journal of Pathology
J Pathol 2024
Published online 17 January 2024 in Wiley Online Library (wileyonlinelibrary.com) DOI: 10.1002/path.6248

ORIGINAL ARTICLE

Dichotomous role of the serine/threonine kinase MAP4K4 in pancreatic ductal adenocarcinoma onset and metastasis through control of AKT and ERK pathways

Amelie Juin[1]*, Heather J Spence[1] and Laura M Machesky[1,2,3]*

[1] *CRUK Beatson Institute, Glasgow, UK*
[2] *School of Cancer Sciences, University of Glasgow, Glasgow, UK*
[3] *Department of Biochemistry, University of Cambridge, Cambridge, UK*

*Correspondence to: A Juin, CRUK Beatson Institute, Garscube Estate, Switchback Road, Bearsden Glasgow G61 1BD, UK. E-mail: a.juin@beatson.gla.ac.uk; LM Machesky, Department of Biochemistry, University of Cambridge, Sanger Building, 80 Tennis Court Road, Cambridge CB2 1GA, UK. E-mail: lmm202@cam.ac.uk

Abstract

MAP4K4 is a serine/threonine kinase of the STE20 family involved in the regulation of actin cytoskeleton dynamics and cell motility. It has been proposed as a target of angiogenesis and inhibitors show potential in cardioprotection. MAP4K4 also mediates cell invasion *in vitro*, is overexpressed in various types of cancer, and is associated with poor patient prognosis. Recently, MAP4K4 has been shown to be overexpressed in pancreatic cancer, but its role in tumour initiation, progression, and metastasis is unknown. Here, using the *Kras*^{G12D} *Trp53*^{R172H} *Pdx1*-Cre (KPC) mouse model of pancreatic ductal adenocarcinoma (PDAC), we show that deletion of *Map4k4* drives tumour initiation and progression. Moreover, we report that the acceleration of tumour onset is also associated with an overactivation of ERK and AKT, two major downstream effectors of KRAS, *in vitro* and *in vivo*. In contrast to the accelerated tumour onset caused by loss of MAP4K4, we observed a reduction in metastatic burden with both the KPC model and in an intraperitoneal transplant assay indicating a major role of MAP4K4 in metastatic seeding. In summary, our study sheds light on the dichotomous role of MAP4K4 in the initiation of PDAC onset, progression, and metastatic dissemination. It also identifies MAP4K4 as a possible druggable target against pancreatic cancer spread, but with the caveat that targeting MAP4K4 might accelerate early tumorigenesis.

Keywords: MAP4K4; pancreatic cancer; invasion; metastatic seeding; pancreatic intraepithelial neoplasia; ERK and AKT signalling pathways

Received 18 May 2023; Revised 24 October 2023; Accepted 4 December 2023

No conflicts of interest were declared.

Introduction

Pancreatic ductal adenocarcinoma (PDAC) is a one of the most fatal malignancies, with a dismal 5-year survival rate of 9% [1,2]. It is a very aggressive cancer, and with a lack of appropriate diagnosis, patients are left with very few treatment options. Despite improvements of chemotherapies and surgical techniques, the 5-year survival rate has not substantially improved in decades [3]. Therefore, understanding the molecular mechanisms inducing the formation of acinar-to-ductal metaplasia (ADM) its progression into pancreatic intraepithelial neoplasia (PanIN) and eventually PDAC is of utmost importance.

Most PDACs are driven by the activation of the oncogene *KRAS*, mainly *KRAS*^{G12D} [4]. RAS signalling plays a major role in pancreatic cancer initiation and maintenance as it drives the activation of two major effector pathways: RAF/MAP kinase (MEK)/ERK and PI3K-AKT pathways [3].

The KPC model, driven by the expression of KRAS^{G12D} and p53^{R172H} (*Trp53*^{R172H}) mutants, is a well-established mouse model of PDAC. It has the advantage of being clinically relevant and recapitulates the key features observed in human PDAC [5]. The RAF–MEK–ERK and PI3K–AKT pathways are frequently activated in this model, and their activation seems to occur at the early stages of PDAC progression [3,6–10].

MAP4K4, also known as HGK (haematopoietic progenitor kinase/germinal centre kinase-like kinase) or NIK (Nck interacting kinase), is a serine/threonine kinase that belongs to the STE20 family of protein kinases. It is widely expressed across a broad range of tissues [11]. Besides its crucial role during embryonic development [12,13], MAP4K4 is also involved in various biological functions, including insulin regulation [14,15], inflammation [16–21], neurodegeneration [22,23], atherosclerosis [13,24], and cytoskeletal functions [25–27]. MAP4K4 has also been recognised as playing an important

role in cancer. High levels of MAP4K4 were correlated with progression and/or poor prognosis in human colorectal cancer tissues and associated with lymph node metastasis [28], hepatocellular carcinoma [29], lung adenocarcinoma [30], prostate cancer [31], and pancreatic cancer [32,33]. More recently, MAP4K4 has been shown to be positively correlated with increased tumour weight in pancreatic cancer [33].

However, the role of MAP4K4 in tumour initiation, maintenance, and progression remains largely unknown. Here, using a mouse model of PDAC, our study unexpectedly highlights that suppression of MAP4K4 accelerates PDAC onset and progression to endpoint but prevents metastasis and lowers tumour burden. Moreover, we demonstrate that a lack of MAP4K4 induces hyperactivation of ERK and PI3K-AKT pathways *in vitro* and *in vivo*. In addition, we show that MAP4K4 is essential for cell matrix remodelling and metastasis seeding, revealing the surprising dual role during PDAC progression and dissemination.

Materials and methods

Genetically modified PDAC mouse model

All animals were maintained in the Biological Services Unit of the Beatson Institute for Cancer Research following UK Home Office regulations and reported in line with the Animal Research: Reporting of In Vivo Experiments (ARRIVE). The protocols and experiments were approved by the Animal Welfare and Ethical Review Body (AWERB) of the University of Glasgow and performed under a UK Home Office licence to Professor Laura Machesky PE494BE48.

The MKPC model was generated by crossing *Map4k4* flox mice [26] with KPC mice. Mice were genotyped by TransnetYX® (Cordova TN, USA) with *LSL-Kras*^{G12D}, *LSL-Trp53*^{R172H}, *Pdx1::CRE* (KPC) mice previously described by Hingorani *et al* [34]. For the survival analysis in Figure 1G, mice were humanely killed when they displayed abdominal swelling or clinical signs consistent with a moderate severity (supplementary material, Table S1). Metastases were generally small and not likely the cause of symptoms, as the size of the primary tumour was by far the majority of the tumour burden.

Generation of cell lines

KPC and MKPC cells were isolated from *LSL-Kras*^{G12D}, *LSL-Trp53*^{R172H}, *Pdx1::CRE* (KPC) or *Map4k4 flox*, *LSL-Kras*^{G12D}, *LSL-Trp53*^{R172H}, *Pdx1-CRE* (MKPC) tumours, as previously described [35]. PDX1 and p53 expression was verified by western blotting. The cells were cultured in DMEM containing 5 g/l glucose, 10% FBS (Gibco, Paisley, UK), 2 mM glutamine (Gibco), and penicillin–streptomycin (Gibco) and maintained at 37 °C under 5% CO_2 in a humidified incubator. PDAC cells were tested regularly for mycoplasma contamination.

Cell proliferation assay

2×10^5 PDAC cells were seeded into six-well plates in triplicate wells. Cells were counted each day for 3 days using a CASY Model TT cell counter (Innovartis, Roche Applied Science, Penzberg, Germany).

Extracellular matrix coating

Glass coverslips were coated with Oregon green 488 conjugate gelatin (G13186, Thermo Fisher Scientific, Waltham, MA, USA) for 10 min, and the excess gelatin was removed using precision wipes (Kimtech Science, Camlab Limited, Cambridge, UK). The coverslips were then inverted on an 80-µl drop of 0.4% glutaraldehyde for 30 min and washed three times with PBS; then 500 µl of 0.4 mg/ml rat tail collagen I (high-concentration collagen I, 354249, Corning, Corning, NY, USA) in D-PBS (σ-Aldrich, Merck KGaA, Darmstadt, Germany) were added on top and incubated for 3 h at 37 °C. After removing the excess of polymerised collagen I fibres, 5×10^4 MKPC expressing mCherry or MAP4K4-mCherry were plated on top of the mixed matrix.

Invasion assays

Invasion assays were performed as previously described [35]. A culture insert (Ibidi, Gräfelfing, Germany) was placed in the middle of a well of a six-well glass bottom dish (MatTek corporation, Ashland, MA, USA), then 6×10^5 PDAC cells were plated around the insert and allowed to settle overnight. The insert and medium were removed, and 350 µl of pure Matrigel were added and left to set for 30 min 37 °C. Before imaging, 3 ml of complete medium was added to the dish. Images were taken every 15 min for 16 h using a Nikon TE2000 microscope with a Plan Fluor ×10/0.30 objective and equipped with a heated CO_2 chamber. Images were analysed with Fiji Software (ImageJ2 version 2.9.0/1.53t (https://imagej.net/software/fiji/downloads).

In vivo PDAC transplantation assays

As previously described [35], 1×10^6 KPC CRISPR CTRL or CRISPR M4K4 #2 cells were washed three times in PBS and then resuspended in 100 µl of PBS. CD-1 nude mice (10 weeks old, Charles River, Tranent, UK) were injected in the i.p. cavity and monitored every day. Mice were humanely sacrificed 2 weeks after injection. Mice were weighed the day of injection and sacrificed.

Immunofluorescence

KPC and MKPC cells were fixed with 4% paraformaldehyde for 15 min at room temperature. Coverslips were then washed three times with PBS and permeabilised with 0.2% Triton X-100 in PBS for 5 min and blocked for 5 min using 4% BSA in PBS. Primary antibodies [anti-Cortactin: 1/250, 05-180, clone 4F11 from Merck Millipore (Burlington, MA, USA), Fish: 1/250, sc-376211,

clone G-7 from Santa Cruz Biotechnology, Dallas, TX, USA] were incubated for 1 h in 4% BSA in PBS and detected using species-specific Alexa488- and Alexa647-conjugated secondary antibodies (1/500, Life Technologies, Thermo Fisher Scientific). DAPI (Sigma-Aldrich) was used to stain nuclei. Coverslips were then mounted with Prolong™ Diamond Antifade Mountant (Invitrogen, Thermo Fisher Scientific). Finally, cells were imaged with a Zeiss 880 Laser Scanning Microscope with Airyscan with a Plan-Apochromat ×63/1.4 oil DIC M27 objective (Zeiss, Oberkochen, Germany).

Immunohistochemistry (IHC)

All haematoxylin and eosin (H&E), Ki67, Cleaved Caspase 3, CK19, p53, CD31, phospho-ERK, α-SMA, and Picro-Sirius red (reagents described in Supplementary materials and methods) staining was performed on 4 µm formalin-fixed paraffin-embedded sections, which had been previously oven baked for 2 h at 60 °C, using standard protocols.

For collagen staining, sections were rehydrated and then immersed in Picro Sirius Red solution (0.1% Direct Red 80, Sigma 41496LH, and 0.1% Fast Green FCF. S142-2, Raymond A Lamb, Durham, NC, USA) for 2 h.

Slides were imaged using a Leica AperioAT2 slide scanner at ×20 magnification and analysed using HALO software (Indica Labs, Albuquerque, NM, USA). Indica Lab algorithm CytoNuclear version 1.6 was used to quantify the number of cells positive for Ki67, Cleaved Caspase 3, and BrdU. The Area Quantification version 1.0 algorithm was used to quantify α-SMA, Picro Sirus Red, and p-ERK staining areas. The intensity staining of p-ERK was categorised as weak with an integrated OD between 0.509 and 0.794, moderate between 0.794 and 0.901, and strong if over 0.901.

Each time, the entire pancreas area on the slide was quantified (~80,000,000 µm^2 per slide) except for the mean vascular density, where the number of CD31$^+$ vessels was manually quantified in 10 fields of view. Each field was >150,000 µm^2.

The percentage areas of normal pancreas, well to poorly differentiated PDAC, and necrosis were quantified manually. We defined as 'necrotic' areas presenting a dissolution of the tissue architecture associated with fragmented nuclei.

PanIN lesion grading was performed on H&E staining according to the architectural abnormalities described in the consensus guidelines published by Hruban *et al* [36].

Statistics and reproducibility

All datasets were analysed using GraphPad Prism 9 (version 9.4.1, GraphPad Software, GraphPad Inc., San Diego, CA, USA). Unless otherwise stated, each experiment was repeated at least three times independently. Differences between groups were tested for normality of distribution (Kolmogorov–Smirnov or Shapiro–Wilk test) and analysed using the appropriate statistical test. Statistical tests used are indicated in each figure legend. p values <0.05 were considered as significant: * $p \le 0.05$, ** $p \le 0.01$, *** $p \le 0.005$.

Results

Map4k4 deletion leads to decreased survival

To investigate the role of MAP4K4 in PDAC progression and dissemination, we crossed *Map4k4* floxed mice into the KPC model of PDAC [5]. We generated *Map4k4 flox; Pdx-1::Cre;LSL-Kras$^{G12D/+}$;LSL-Trp53^{R172H}* (MKPC) mice to specifically knock out *Map4k4* in pancreatic epithelial cells (acini and ducts) (Figure 1A). Western blot analysis of proteins isolated from organoids generated from KPC and MKPC mice confirmed that MAP4K4 protein expression was lost in the pancreas (Figure 1B). Loss of MAP4K4 also did not substantially impact blood glucose, ureas, or triglyceride blood levels at 6 to 15 weeks (supplementary material, Figure S1A–C) and so likely did not have a significant effect on normal pancreatic function. By the endpoint, KPC and MKPC tumours appeared histologically similar (Figure 1C–F and supplementary material, Figure S2A–E) and displayed comparable tumour to body mass ratio (Figure 1D). There was no significant difference in cell proliferation (Figure 1E), but there was significantly less cell death in MKPC tumours (Figure 1F). Moreover, there was no detectable difference in the vascular density or necrosis (supplementary material, Figure S2A,E–G). Looking at the α-SMA expression, MKPC tumours appeared to contain more myofibroblasts than KPC tumours but showed a similar level of fibrillar collagen (stained with Picro Sirius Red, supplementary material, Figure S2A,C). However, MAP4K4 deletion was associated with a highly significant reduction in time to endpoint, indicating more rapid progression of the primary tumours of these mice (Figure 1G). Loss of MAP4K4 also affected PDAC dissemination as MKPC mice showed a trend toward a lower metastasis burden (Figure 1H) and a dramatically reduced number of mice presenting with ascites and reduced fluid volume (supplementary material, Figure S2H,I). Thus, MAP4K4 loss in pancreatic tumours showed an unexpected impact on survival and tumour dissemination.

MAP4K4 deletion accelerates PDAC onset and progression

Given the tight regulation of MAPK signalling during the development of pancreatic intraepithelial neoplasia [37], we next assessed whether MAP4K4 was important for PDAC onset and progression by first assessing the pancreata of KPC and MKPC mice at earlier time points. No differences were observed at 6 weeks in the percentage of mice presenting PDAC foci (Figure 2A,B). However, MKPC mice presented a higher grade of PanIN lesions in comparison to KPC mice (Figure 2E and supplementary material, Figure S2J–L).

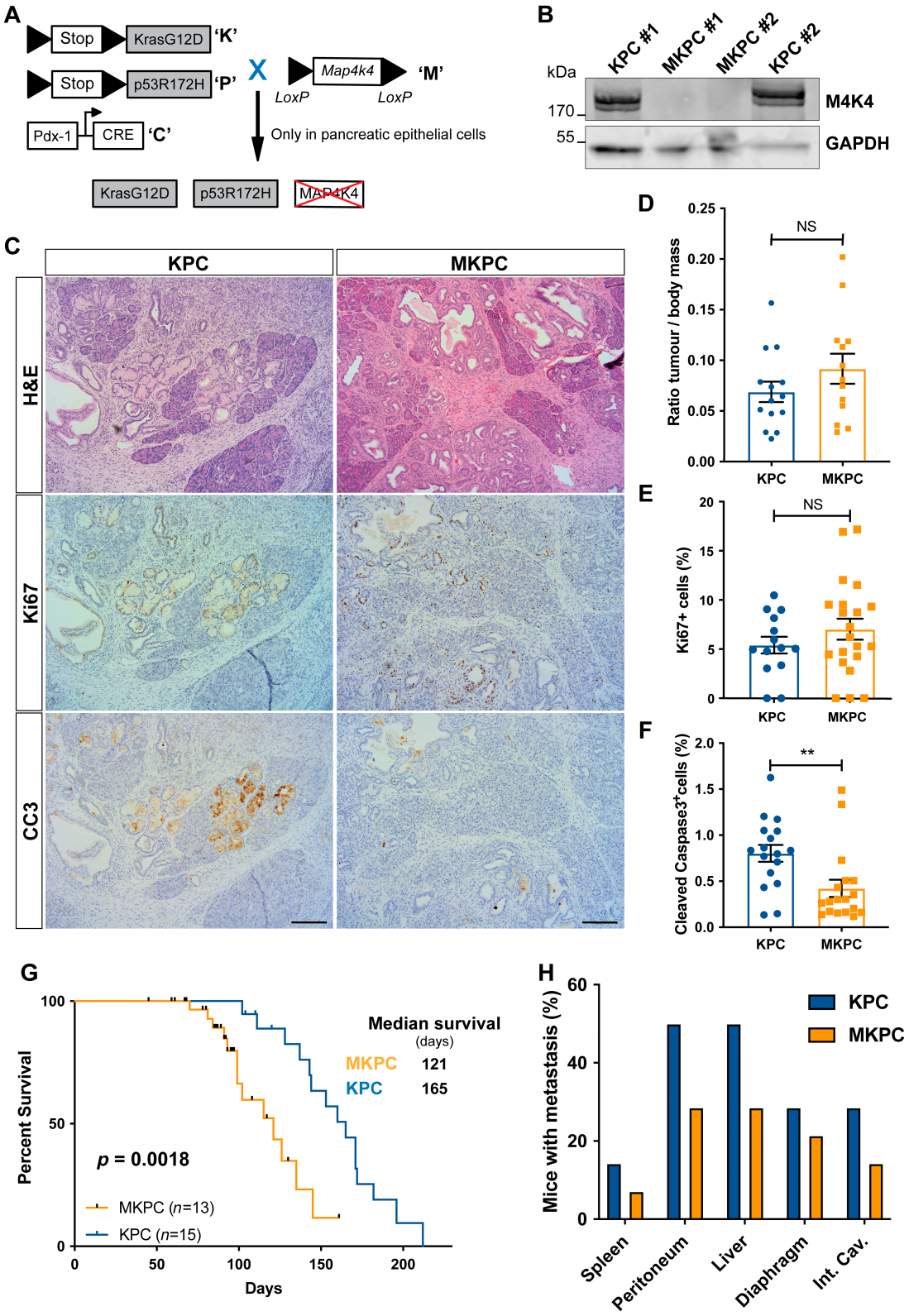

Figure 1. MAP4K4 is required for PDAC dissemination. (A) Genetic strategy to delete *Map4k4* in KPC mice. (B) Western blot panels showing MAP4K4 (M4K4) expression in pancreatic organoids isolated from two independent KPC (KPC #1 and KPC #2) and MKPC (MKPC #1 and MKPC #2) mice. (C) Serial sections of PDAC tumours stained with H&E (top), KI67 (proliferation marker, middle) and cleaved caspase 3 (CC3, apoptosis marker, bottom). Scale bar, 200 ≤ µm. (D) Bar chart showing tumour-to-body weight ratios at sacrifice. Mean ± SEM (n = 14 KPC and 13 MKPC mice, unpaired t-test with Welch's correction, non-significant). (E and F) Quantification of Ki67$^+$ and CC3$^+$ cells in PDAC tumours from KPC and MKPC mice. Mean ± SEM, for Ki67 quantification: n = 14 KPC (over 11,798 cells quantified per slide) and 21 MKPC mice (over 15,586 cells quantified per slide), unpaired t-test with Welch's correction, non-significant; for CC3 quantification: n = 17 KPC (over 22,702 cells quantified per slide) and 18 MKPC mice (over 19,475 cells quantified per slide), Mann–Whitney test, $^{**}p \leq 0.01$. (G) Kaplan–Meier survival analysis showing survival in KPC and KPC *Map4k4*−/− mice. (n = 15 KPC and 13 MKPC mice, Gehan–Breslow–Wilcoxon test). (H) Incidence and localisation of KPC and MKPC metastasis. (Int. cav., intraperitoneal cavity)

This was also associated with an increased proliferation of the PanIN areas (Figure 2A,F,G). By 10 weeks, five out of five MKPC versus zero out of five KPC mice showed PDAC foci (Figure 2B) and *Map4k4* deleted pancreata presented a significant replacement of the normal ducts by PanIN lesions

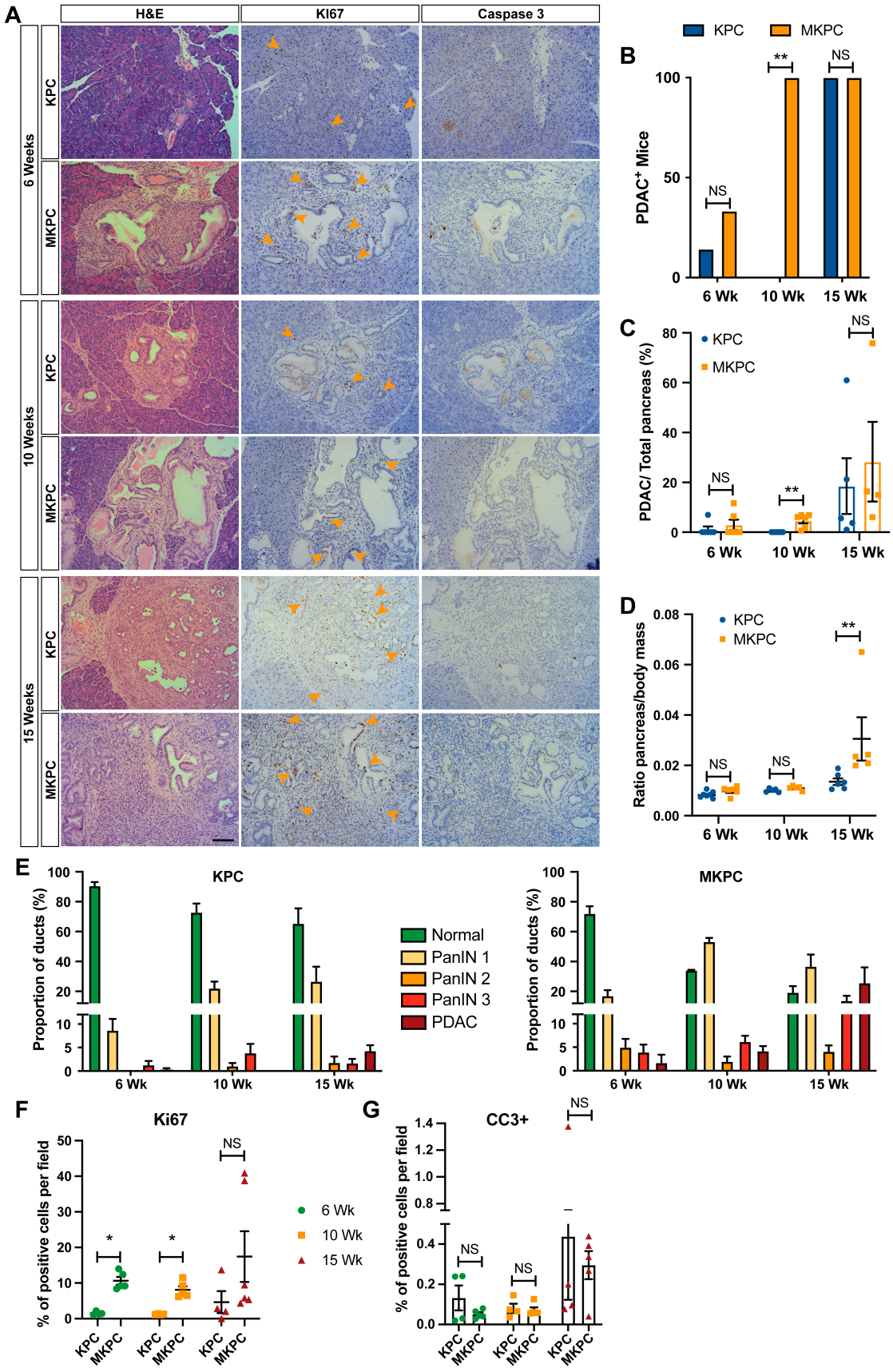

Figure 2 Legend on next page.

(Figure 2E and supplementary material, Figure S2K). This was also correlated with a significant increase of the relative tumour size (Figure 2C) and tumour growth (Figure 2D). At 15 weeks, both KPC and MKPC mice presented with higher grade PanIN lesions (Figure 2E and supplementary material, Figure S2L) and small PDAC foci (Figure 2A,B), but to a greater extent in MKPC mice. At this time point, the gradual progression to advanced PanIN lesions and PDAC foci formation correlated to an increased tumour-over-body mass ratio in MKPC mice. Concomitantly to the replacement of normal pancreatic tissue and tumour progression, lower blood serum levels of amylase and lipase were identified at 15 weeks in MKPC mice (supplementary material, Figure S1D–E). Together, these data indicate that *Map4k4* deletion accelerates the development of pancreatic intraepithelial neoplasia lesions and PDAC progression.

MAP4K4 is required for invasion and metastatic seeding

To investigate the mechanisms by which MAP4K4 promotes metastasis, we deleted *Map4k4* from a cell line made from a KPC mouse tumour (KPC cells) using CRISPR. MKPC cells were also isolated from MKPC tumour-bearing mouse and either labelled with mCherry or rescued with MAP4K4-mCherry (supplementary material, Figure S3A,B). As MAP4K4 shows some sequence homology with MAP4K5 and especially with MAP4K6 (also known as MINK1), the protein levels of other MAP4Ks, MAP4K5, and MAP4K6, were assessed. Knockout of MAP4K4 did not trigger a compensation of these kinases (supplementary material, Figure S3C–F). Using circular invasion assays [38], we challenged the invasiveness of MKPC cells through Matrigel and observed that MAP4K4-depleted cells were significantly less invasive (Figure 3A,B). PDAC presents an extracellular matrix highly enriched in fibrillar collagens. To determine whether MAP4K4 was important for matrix remodelling and degradation, we cultured MAP4K4 rescued (M4K4-mCherry) and knockout cells (mCherry) on a mixed matrix of gelatin and collagen I fibres. We noticed that collagen I fibres promoted the formation of linear invadosomes in both cell lines (supplementary material, Figure S4A,B). However, rescued cells showed significantly more gelatin degradation than mCherry MKPC cells, suggesting a role for MAP4K4 in matrix remodelling and degradation (Figure 3C,D).

To further characterise the specificity of MAP4K4 function in metastatic seeding, we performed intraperitoneal injection experiments. These experiments directly address whether MAP4K4 has a role in metastatic seeding and clarify whether the metastatic impairment in the MKPC mice was likely just due to the animals reaching endpoint sooner due to the primary tumour burden. Control and MAP4K4 #2 CRISPR KPC cells, which present a similar level of proliferation (supplementary material, Figure S4C), were injected into the i.p. cavity of nude mice. We observed that 80% of mice injected with Control CRISPR KPC cells presented with jaundice (Figure 3F) and a loss of weight (Figure 3G), two usual symptoms reminiscent of the human PDAC disease. Mice injected with MAP4K4 CRISPR KPC cells showed no spleen invasion, the incidence of liver tumour was lower and, in general, displayed fewer and less invasive metastatic nodules (Figure 3E,F,H,I). These data demonstrate that MAP4K4 plays an essential role during PDAC invasion and metastatic seeding.

Map4k4 deletion promotes an overactivation of AKT and ERK pathways

To identify the mechanisms by which MAP4K4 drives PDAC tumorigenesis, we investigated the functional interplay between MAP4K4 and signalling pathways frequently activated during pancreatic intraepithelial neoplasia development [10,37,39]. We analysed the activation of the PI3K–AKT and ERK pathways in mCherry and MAP4K4-mCherry rescued MKPC cells upon serum stimulation. Using specific phospho-antibodies and western blotting, we observed that both knockout and MAP4K4 rescued cells showed an increase in the

Figure 2. A loss of MAP4K4 accelerates PDAC progression. (A) Representative serial sections of H&E, Ki67, and cleaved caspase 3 staining of pancreata from 6 weeks (top section), 10 weeks (middle section) and 15 weeks (bottom section) aged KPC (top panel) and MKPC (bottom panel) mice. Orange arrowheads represent KI67$^+$ cells. Scale bar, 200 µm. (B) Incidence of PDAC in 6, 10, and 15 weeks KPC and MKPC mice ($n = 5$ KPC and 5 MKPC mice). Incidence is expressed as a percentage of PDAC$^+$ mice, Fisher's exact test, $^{**}p \leq 0.01$. (C) Percentage of PDAC area normalised to the total pancreatic area at indicated times. Mean ± SEM, at 6 weeks $n = 6$ KPC and 6 MKPC mice, at 10 weeks $n = 5$ KPC and 5 MKPC mice and 15 weeks $n = 5$ KPC and 4 MKPC mice, Mann–Whitney test, $^{**}p \leq 0.01$. (D) Scatter plots showing tumour-to-body mass ratios at 6, 10, and 15 weeks. Mean ± SEM, at 6 weeks, $n = 7$ KPC and 6 MKPC mice, at 10 weeks $n = 5$ KPC and 5 MKPC mice and 15 weeks $n = 5$ KPC and 5 MKPC mice, Mann–Whitney test, $^{**}p \leq 0.01$. (E) Bar chart showing PDAC neoplastic progression of KPC and MKPC mice at indicated times. At 6 weeks $n = 5$ KPC (normal ducts: 188, PanIN 1: 21, PanIN 2: 0, PanIN 3: 2, PDAC lesion: 1), and 5 MKPC mice (normal ducts: 130, PanIN 1: 33, PanIN 2: 9, PanIN 3: 8, PDAC lesion: 3); at 10 weeks $n = 5$ KPC (normal ducts: 170, PanIN 1: 51, PanIN 2: 2, PanIN 3: 11, PDAC lesion: 0) and 5 MKPC mice (normal ducts: 179, PanIN 1: 233, PanIN 2: 8, PanIN 3: 26, PDAC lesion: 17); at 15 weeks $n = 3$ KPC (normal ducts: 168, PanIN 1: 81, PanIN 2: 7, PanIN 3: 6, PDAC lesion: 11) and 4 MKPC mice (normal ducts: 113, PanIN 1: 243, PanIN 2: 25, PanIN 3: 78, PDAC lesion: 141). Mean ± SEM. Statistics are presented in supplementary material, Figure S2J,K. (F and G) Quantification of percentage of Ki67$^+$ and cleaved caspase 3$^+$ cells per field of view. Mean ± SEM, at 6 weeks: $n = 4$ KPC (for KI67 and CC3, respectively, over 194,370 and 240,677 cells were quantified per slide) and 5 MKPC mice (for KI67 and CC3, respectively, over 119,248 and 235,441 cells were quantified per slide); at 10 weeks $n = 4$ KPC (for Ki67 and CC3, respectively, over 184,295 and 301,071 cells were quantified per slide) and 5 MKPC mice (for Ki67 and CC3, respectively, over 174,076 and 427,645 cells were quantified per slide); at 15 weeks for Ki67 $n = 4$ KPC (for Ki67 and CC3, respectively, over 221,434 and 440,801 cells were quantified per slide) and 6 MKPC mice (for Ki67 and CC3, respectively, over 177,734 and 182,879 cells were quantified per slide), Mann–Whitney test, $^{*}p \leq 0.05$.

phosphorylation of AKT and ERK pathways upon serum stimulation (Figure 4A–C). MAP4K4 knockout cells presented significantly higher AKT and ERK phosphorylation levels in the presence of serum in comparison to rescued cells (Figure 4A–C). We also noted that the phospho-AKT level was significantly higher in

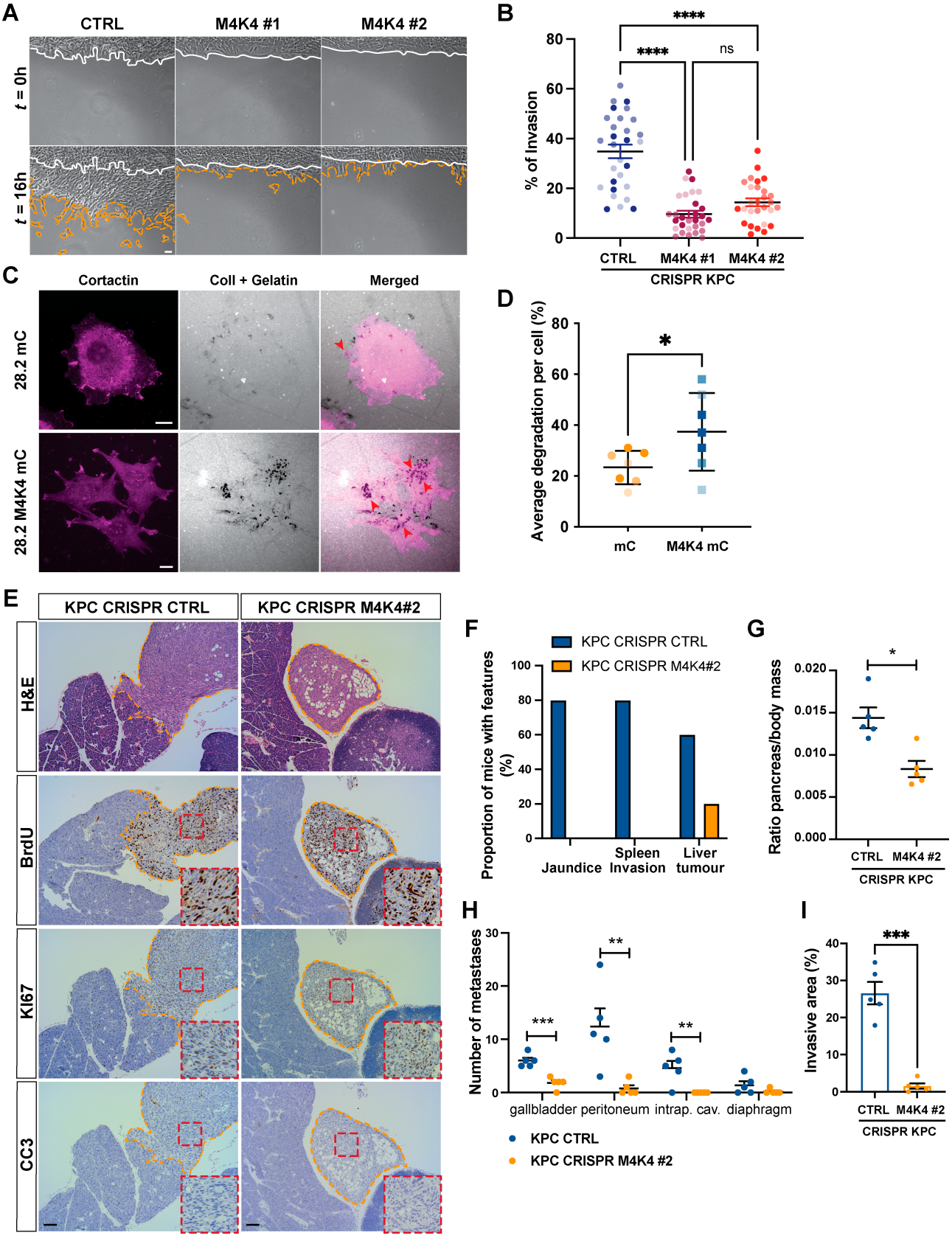

Figure 3 Legend on next page.

serum-free conditions. However, no differences were observed in the phosphorylation levels of YAP, p38, and JNK, pathways previously shown to be regulated by MAP4K4 (supplementary material, Figure S5A–D) [18,40–44]. Furthermore, the AKT and ERK total protein levels were not affected by a loss of MAP4K4 (supplementary material, Figure S5F–H). To confirm that MAP4K4 contributes to AKT and ERK activation, we used an inhibitor of MAP4K4 kinase activity, PF06260933. MAP4K4 rescued cells treated with the inhibitor showed AKT and ERK phosphorylation levels similar to those of the knockout cells, confirming that the kinase activity of MAP4K4 was essential to activate these pathways (supplementary material, Figure S6A–C).

We also observed a higher level of phosphorylation of mTOR^{S2448} in MAP4K4-depleted cells (supplementary material, Figure S5A,E). This trend prompted us to investigate whether a lack of MAP4K4 could influence the phosphorylation of mTORC1 and mTORC2 downstream effectors. Western blot analysis revealed that both the downstream target of mTORC1 (phospho-P70S6K^{Thr398}, Figure 4A,D) and subunits of the mTORC2 complex (phospho-Sin1^{Thr86} and phospho-RICTOR^{Thr1135}, Figure 4A,E,F) were clearly increased in MAP4K4 knockout cells. This was also correlated with a strong and sustained phosphorylation of an upstream target of the PI3K/AKT pathway, the EGF receptor (EGFR) (Figure 4A,G), in mCherry MKPC cells. However, it appeared that a lack of MAP4K4 did not affect the total level of EGFR and RICTOR (supplementary material, Figure S5F,I,J). These results demonstrate that a lack of MAP4K4 induces the hyperactivation of ERK and EGFR/AKT/mTOR pathways in cells expressing KRAS^{G12D}.

MAP4K4 loss enhances ERK activity during PDAC progression

To further investigate the mechanisms by which a loss of MAP4K4 could facilitate PDAC onset, histological sections of pancreas from KPC and MKPC mice at 6, 10, and 15 weeks were stained with phospho-ERK to validate the *in vitro* observations. At 6 and 10 weeks, we observed that mostly PanIN lesions and ducts were weakly stained with phospho-ERK$^{Thr202/Tyr204}$, confirming that the ERK pathway was activated. No difference was noticed in the percentage of phospho-ERK staining over the total surface of the pancreas (Figure 5A,B) or the staining intensity (Figure 5C) at these times. However, at 15 weeks, MKPC tumours tended to present a wider area stained for phospho-ERK$^{Thr202/Tyr204}$ as well as a higher moderate and high phospho-ERK$^{Thr202/Tyr204}$ staining intensity (Figure 5A–C). Taken together, these data demonstrate that loss of MAP4K4 tends to also induce hyperactivation of the ERK pathway *in vivo* during PDAC onset.

Discussion

MAP4K4 is a serine/threonine kinase that is overexpressed in a variety of cancers and associated with poor prognosis. It has been reported that MAP4K4 is overexpressed in the late stage of pancreatic tumorigenesis [32,33], although its role during PDAC initiation and progression is unknown. The development of tools such as inhibitors of MAP4K4 suggested a potential window of opportunity to explore the importance of this target in pancreatic cancer. Given a large literature implicating MAP4K4 in cell migration and invasion, we sought to determine whether eliminating MAP4K4 in a genetic model of pancreatic cancer would prevent metastatic dissemination of tumours and suggest a potential therapeutic angle for this highly metastatic cancer.

In this study, using the classic *flox;Pdx-1::Cre;LSL-Kras$^{G12D/+}$;LSL-p53^{R172H}* KPC model [5], we demonstrated the pivotal and unanticipated role of MAP4K4 in PDAC initiation and progression. Strikingly, we observed that MAP4K4 deletion caused an acceleration of PDAC onset with higher grades of PanIN in MKPC mice early on, suggesting that MAP4K4 might be crucial to promote PDAC development. Interestingly, MAP4K4 regulates cytoskeleton dynamics and cell motility.

Figure 3. MAP4K4 is required for invasion *in vitro* and is driving metastatic seeding *in vivo*. See supplementary material, Figure S3A for a table explaining the nomenclature of cell lines. (A) Invasion assay showing representative images of CTRL or MAP4K4 independently generated CRISPR KPC cells (M4K4 #1 and M4K4 #2) at $t = 0$ h or $t = 16$ h after invading Matrigel. Scale bar, 200 µm. White lines indicate starting point cell edges. Orange lines indicate invasive edge at 16 h. (B) Scatter plots showing percentage of invasion. Mean ± SEM, $n = 3$ independent experiments with $n > 8$ fields of view quantified each time. Each experiment is colour coded. One-way ANOVA with Kruskal–Wallis multiple comparison test, $^{***}p \le 0.001$ and $^{****}p \le 0.0001$. (C) Representative confocal images of mCherry (top panel, 28.2 mC) and MAP4K4-mCherry rescue (bottom panel, 28.2 M4K4 mC) cells seeded on a mixed collagen I/FITC-gelatin matrix. Red arrowheads show colocalisation between Cortactin (magenta) and degraded matrix (grey) at linear invadosomes. Scale bar, 10 µm. (D) Scatter plot showing average percentage of collagen I/FITC-gelatin mix degradation per cell. Mean ± SEM, $n = 3$ independent experiments, each time two or three distinct fields of view were quantified. Each field of view had a minimum of 10 cells. Each experiment is colour coded. Unpaired *t*-test, $^{*}p \le 0.05$. (E) Representative H&E (top panel), BrdU (top middle), Ki67 (bottom middle), and cleaved caspase 3 (bottom) images of pancreas of nude mice i.p. injected with CTRL or MAP4K4 #2 CRISPR KPC cells. Scale bar, 200 µm. Orange dotted line indicates tumour outline. Red insets show greater magnifications of positive cells. (F) Incidence (%) of mice with jaundice, spleen invasion, or liver tumour. (G) Scatter plots showing pancreas-to-body weight ratio at sacrifice. Mean ± SEM, $n = 5$ CTRL CRISPR KPC and $n = 5$ MAP4K4 #2 CRISPR KPC mice, Mann–Whitney test, $^{*}p \le 0.05$. (H) Scatter plots showing number of metastases on gallbladder, peritoneum, diaphragm, and in i.p. cavity. Mean ± SEM, $n = 5$ CTRL CRISPR KPC and $n = 5$ MAP4K4 #2 CRISPR KPC mice, multiple *t*-tests, $^{**}p \le 0.01$ and $^{***}p \le 0.001$. (I) Quantification of invasive area by CTRL or MAP4K4 #2 CRISPR KPC cells. Orange dotted lines represent limit of invasive front. Mean ± SEM, $n = 5$ CTRL CRISPR KPC and $n = 5$ MAP4K4 #2 CRISPR KPC mice, Welch's *t*-test, $^{***}p \le 0.001$.

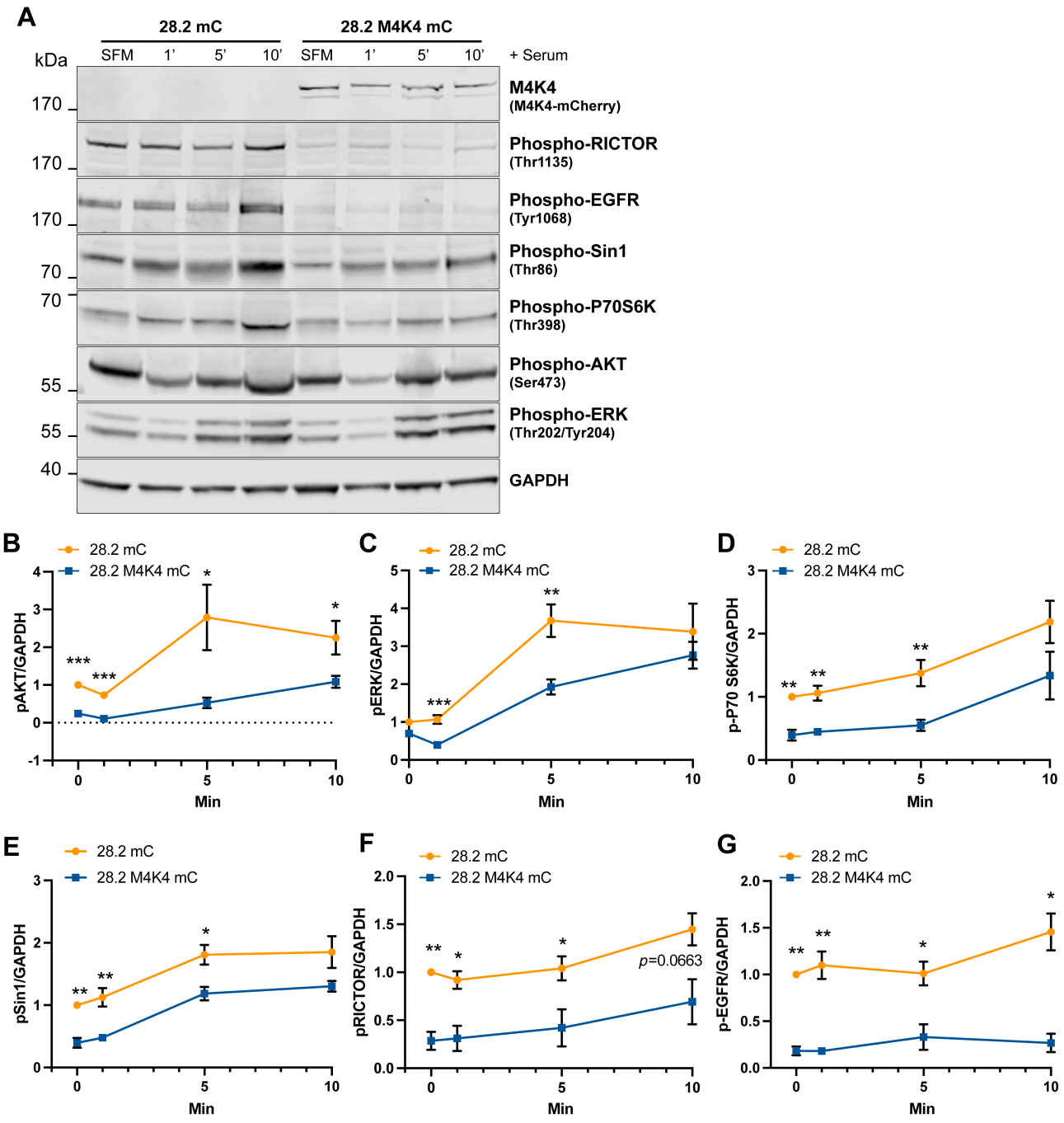

Figure 4. MAP4K4 depletion induces activation of AKT, ERK, and mTORC signalling pathways. (A) Phosphorylation levels of RICTOR, EGF receptor, Sin1, P70 S6K, AKT, and ERK were measured by immunoblotting after serum stimulation at indicated times. GAPDH is a sample integrity control. Blots are representative of five experiments. SFM, serum-free medium. Cell nomenclature is described in supplementary material, Figure S3A. (B–G) Densitometric quantification of proteins in panel (a) at indicated times. Mean ± SEM. Statistical significance was assessed using Mann–Whitney tests or Welch's *t*-tests as required for each time point; $^{*}p \leq 0.05$, $^{**}p \leq 0.01$, $^{***}p \leq 0.001$.

In particular, it directly interacts with the ERM proteins [45] and promotes the destabilisation of focal adhesions by activation of Arf6 through its interaction with EB2 [27]. ERM proteins and Arf6 have been described to be involved in the organisation of the apical actin cytoskeleton in epithelial cells [46–48]. Likewise, EB2 is essential for microtubule reorganisation during epithelial polarisation [49]. During ADM, acinar cells change morphology and lose polarity [50]. Thus, loss of MAP4K4 could lead to a polarity defect in acinar cells and, consequently, an acceleration of tumour onset. To improve the understanding of the role of MAP4K4 in the apico-basal polarity in acini, future studies could explore the potential pathways involved using pancreatic organoids isolated from MKPC mice.

Our data revealed that at 15 weeks, MKPC pancreata showed a higher level of phospho-ERK, a downstream effector of KRAS important for both initiation and maintenance of pancreatic lesions [3]. Using MKPC cells extracted from tumour-bearing mice, we

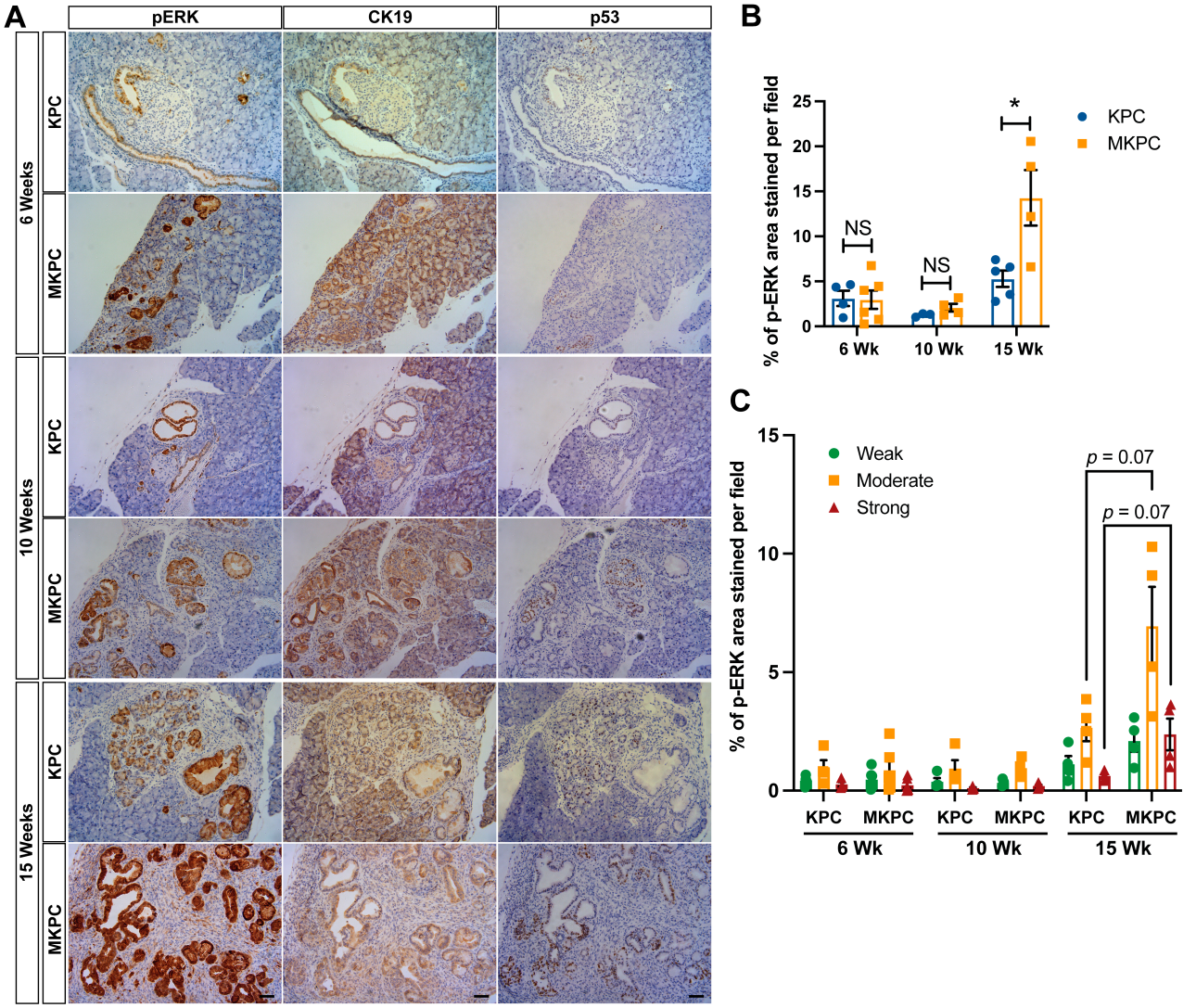

Figure 5. PDAC progression is associated with a modestly higher level of phospho-ERK in MKPC pancreata. (A) Representative histological images of 6 weeks (top section), 10 weeks (middle section), and 15 weeks (bottom section) pancreata from KPC and MKPC mice stained with phospho-ERK, CK19, and p53. Scale bar, 200 μm. (B) Quantification of phospho-ERK expression in pancreas of mice at indicated time points. Data are presented as percentage of total stained area per field. Mean ± SEM, at 6 weeks, $n = 4$ KPC and 6 MKPC mice; at 10 weeks $n = 3$ KPC and 4 MKPC mice and 15 weeks $n = 5$ KPC and 4 MKPC mice, unpaired t-test, $^*p \leq 0.05$. (C) Differential expression of phospho-ERK in pancreas of mice at indicated time point. Data are presented as percentage of total stained area per field. Mean ± SEM, at 6 weeks, $n = 4$ KPC and 6 MKPC mice; at 10 weeks and 15 weeks $n = 4$ KPC and 4 MKPC mice, unpaired t-test.

demonstrated hyperactivation of the ERK and PI3K-AKT pathways. In our study, it also appeared that targeting MAP4K4 in KPC cells, with the inhibitor PF06260933, also promoted high ERK and AKT phosphorylation levels similar to what we observed in MKPC cells. Our findings are consistent with recent studies showing elevated phosphorylation of ERK [18,20] or AKT in MAP4K4-depleted cells or tissues [15,51]. mTORC1 and mTORC2 signalling has also been linked to promote PDAC onset, progression, and dissemination [39,52,53]. In MKPC cells, we demonstrated a high level of activation of mTORC1 and mTORC2, in line with these data. In summary, we propose that the high level of phosphorylation of ERK and AKT, two essential KRAS effectors, as well as downstream effectors in MKPC pancreata could facilitate the acceleration of PDAC onset. Thus, these findings highlight a potential significance of MAP4K4's mechanistic role in promoting the initiation of PDAC.

Of note, the activation of JNK cascade and Hippo pathway were not affected in our system. We speculate this could be explained by distinct and/or tissue-/cell-specific regulation by MAP4K4 [20,22,25,40,41,54–57].

By the endpoint, KPC and MKPC tumours had similar histological features in terms of proliferation rate and appearance of the tumour extracellular matrix components. Interestingly, MAP4K4 inhibition has been linked to an increase of apoptosis in pancreatic cancer cells [33]. However, we noticed a slight decrease of cell death rate in MKPC tumours. This result could be explained by the protective effect from cell death of the dense stromal microenvironment.

Interestingly, metastases were reduced in both the KPC model and i.p. transplantation assays demonstrating

that MAP4K4 controlled metastatic seeding *in vivo*. Our data are in line with several studies reporting the important role of MAP4K4 in invasion and migration [58,59]. We recently published a paper showing pancreatic cancer cells exhibit chemotaxis towards lysophosphatidic acid (LPA) and that N-WASP controls trafficking driving invasion [35]. In particular, a loss of N-WASP induced the aberrant recycling of LPAR1 receptor. Given the fact that MAP4K4 is a major regulator of endocytosis and trafficking to focal adhesion sites [26,27,60], we could hypothesise that receptor tyrosine kinases, G protein-coupled receptors, and/or integrins are not internalised adequately in MAP4K4 knockout cells. This would lead to an excessive activation of downstream signalling pathways and reduced migration/invasion capacities in MAP4K4 null cells, explaining our data.

Small molecule inhibitors have been designed to target the oncogenic properties of MAP4K4. One such compound, bosutinib, used for the treatment of chronic myeloid leukaemia [61], has shown encouraging results at stabilising the endothelial barrier and, thus, preventing vascular leakage in mice [57]. However, given our present study showing that a loss of MAP4K4 accelerates PDAC onset and progression, the use of pharmaceutical inhibitor of MAP4K4 would require careful evaluation before undertaking clinical trials for solid tumour cancers. It would be interesting to perform preclinical treatments of mice with bosutinib to determine whether this also caused an acceleration of tumour progression and/or inhibited metastasis to distant sites.

In summary, our work highlights the dichotomous role of MAP4K4 in the initiation of PanIN lesions and PDAC progression and its distinct function during metastatic dissemination. The rapid progression towards PDAC is attributed to the hyperactivation of two major KRAS-driven pathways, ERK and AKT, which are demonstrated *in vivo* for ERK and *in vitro* for both ERK and AKT. The pharmaceutical inhibition of MAP4K4 could be of therapeutic interest to target PDAC metastases in cancer patients, but with a cautionary note that it could accelerate tumour progression.

Acknowledgements

We would like to express our gratitude to Dr Weilan Ye from Genentech for the MAP4K4 flox mice, Colin Nixon and the Beatson Histology Services, all the staff at Biological Service Unit and Biological Research Unit, and the Beatson Advanced Imaging Resource (BAIR) imaging facility. LMM was funded by Cancer Research UK core grants to the Beatson Institute (A17196, A31287, and A24452).

Author contributions statement

AJ and LMM conceived and designed the study. AJ and HJS performed data collection and analysed the data. AJ and LMM wrote the manuscript. All the authors approved the final version of the manuscript for publication.

Data availability statement

Data sharing not applicable to this article as no datasets were generated or analysed during the current study.

References

1. Rawla P, Sunkara T, Gaduputi V. Epidemiology of pancreatic cancer: global trends, etiology and risk factors. *World J Oncol* 2019; **10:** 10–27.
2. Sung H, Ferlay J, Siegel RL. Global cancer statistics 2020: GLOBOCAN estimates of incidence and mortality worldwide for 36 cancers in 185 countries. *CA Cancer J Clin* 2021; **71:** 209–249.
3. Wang S, Zheng Y, Yang F, *et al*. The molecular biology of pancreatic adenocarcinoma: translational challenges and clinical perspectives. *Signal Transduct Target Ther* 2021; **6:** 249.
4. Jones S, Zhang X, Parsons DW, *et al*. Core signaling pathways in human pancreatic cancers revealed by global genomic analyses. *Science* 2008; **321:** 1801–1806.
5. Hingorani SR, Wang L, Multani AS, *et al*. Trp53R172H and KrasG12D cooperate to promote chromosomal instability and widely metastatic pancreatic ductal adenocarcinoma in mice. *Cancer Cell* 2005; **7:** 469–483.
6. Collisson EA, Trejo CL, Silva JM, *et al*. A central role for RAF→MEK→ERK signaling in the genesis of pancreatic ductal adenocarcinoma. *Cancer Discov* 2012; **2:** 685–693.
7. Elghazi L, Weiss AJ, Barker DJ, *et al*. Regulation of pancreas plasticity and malignant transformation by Akt signaling. *Gastroenterology* 2009; **136:** 1091–1103.
8. Alliouachene S, Tuttle RL, Boumard S, *et al*. Constitutively active Akt1 expression in mouse pancreas requires S6 kinase 1 for insulinoma formation. *J Clin Invest* 2008; **118:** 3629–3638.
9. Eser S, Reiff N, Messer M, *et al*. Selective requirement of PI3K/PDK1 signaling for Kras oncogene-driven pancreatic cell plasticity and cancer. *Cancer Cell* 2013; **23:** 406–420.
10. Albury TM, Pandey V, Gitto SB, *et al*. Constitutively active Akt1 cooperates with KRas(G12D) to accelerate in vivo pancreatic tumor onset and progression. *Neoplasia* 2015; **17:** 175–182.
11. Wright JH, Wang X, Manning G, *et al*. The STE20 kinase HGK is broadly expressed in human tumor cells and can modulate cellular transformation, invasion, and adhesion. *Mol Cell Biol* 2003; **23:** 2068–2082.
12. Xue Y, Wang X, Li Z, *et al*. Mesodermal patterning defect in mice lacking the Ste20 NCK interacting kinase (NIK). *Development* 2001; **128:** 1559–1572.
13. Roth Flach RJ, Guo C-A, Danai LV, *et al*. Endothelial mitogen-activated protein kinase kinase kinase kinase 4 is critical for lymphatic vascular development and function. *Mol Cell Biol* 2016; **36:** 1740–1749.
14. Tang X, Guilherme A, Chakladar A, *et al*. An RNA interference-based screen identifies MAP4K4/NIK as a negative regulator of PPARgamma, adipogenesis, and insulin-responsive hexose transport. *Proc Natl Acad Sci U S A* 2006; **103:** 2087–2092.
15. Danai LV, Roth Flach RJ, Virbasius JV, *et al*. Inducible deletion of protein kinase Map4k4 in obese mice improves insulin sensitivity in liver and adipose tissues. *Mol Cell Biol* 2015; **35:** 2356–2365.

16. Aouadi M, Tesz GJ, Nicoloro SM, *et al*. Orally delivered siRNA targeting macrophage Map4k4 suppresses systemic inflammation. *Nature* 2009; **458:** 1180–1184.
17. Jin M, Chu H, Li Y, *et al*. MAP4K4 deficiency in CD4(+) T cells aggravates lung damage induced by ozone-oxidized black carbon particles. *Environ Toxicol Pharmacol* 2016; **46:** 246–254.
18. Bouzakri K, Zierath JR. MAP4K4 gene silencing in human skeletal muscle prevents tumor necrosis factor-alpha-induced insulin resistance. *J Biol Chem* 2007; **282:** 7783–7789.
19. Chuang HC, Sheu WH-H, Lin Y-T, *et al*. HGK/MAP4K4 deficiency induces TRAF2 stabilization and Th17 differentiation leading to insulin resistance. *Nat Commun* 2014; **5:** 4602.
20. Chuang HC, Wang X, Tan TH. MAP4K family kinases in immunity and inflammation. *Adv Immunol* 2016; **129:** 277–314.
21. Esen E, Sergin I, Jesudason R, *et al*. MAP4K4 negatively regulates CD8 T cell-mediated antitumor and antiviral immunity. *Sci Immunol* 2020; **5:** eaay2245.
22. Larhammar M, Huntwork-Rodriguez S, Rudhard Y, *et al*. The Ste20 family kinases MAP4K4, MINK1, and TNIK converge to regulate stress-induced JNK signaling in neurons. *J Neurosci* 2017; **37:** 11074–11084.
23. Wu C, Watts ME, Rubin LL. MAP4K4 activation mediates motor neuron degeneration in amyotrophic lateral sclerosis. *Cell Rep* 2019; **26:** 1143–1156.e5.
24. Fiedler LR, Chapman K, Xie M, *et al*. MAP4K4 inhibition promotes survival of human stem cell-derived cardiomyocytes and reduces infarct size in vivo. *Cell Stem Cell* 2019; **24:** 458.
25. Collins CS, Hong J, Sapinoso L, *et al*. A small interfering RNA screen for modulators of tumor cell motility identifies MAP4K4 as a promigratory kinase. *Proc Natl Acad Sci U S A* 2006; **103:** 3775–3780.
26. Vitorino P, Yeung S, Crow A, *et al*. MAP4K4 regulates integrin-FERM binding to control endothelial cell motility. *Nature* 2015; **519:** 425–430.
27. Yue J, Xie M, Gou X, *et al*. Microtubules regulate focal adhesion dynamics through MAP4K4. *Dev Cell* 2014; **31:** 572–585.
28. Hao JM, Chen J-Z, Sui H-M, *et al*. A five-gene signature as a potential predictor of metastasis and survival in colorectal cancer. *J Pathol* 2010; **220:** 475–489.
29. Liu AW, Cai J, Zhao X-L, *et al*. ShRNA-targeted MAP4K4 inhibits hepatocellular carcinoma growth. *Clin Cancer Res* 2011; **17:** 710–720.
30. Qiu MH, Qian Y-M, Zhao X-L, *et al*. Expression and prognostic significance of MAP4K4 in lung adenocarcinoma. *Pathol Res Pract* 2012; **208:** 541–548.
31. Rizzardi AE, Rosener NK, Koopmeiners JS, *et al*. Evaluation of protein biomarkers of prostate cancer aggressiveness. *BMC Cancer* 2014; **14:** 244.
32. Liang JJ, Wang H, Rashid A, *et al*. Expression of MAP4K4 is associated with worse prognosis in patients with stage II pancreatic ductal adenocarcinoma. *Clin Cancer Res* 2008; **14:** 7043–7049.
33. Singh SK, Kumar S, Viswakarma N, *et al*. MAP4K4 promotes pancreatic tumorigenesis via phosphorylation and activation of mixed lineage kinase 3. *Oncogene* 2021; **40:** 6153–6165.
34. Hingorani SR, Petricoin EF, Maitra A, *et al*. Preinvasive and invasive ductal pancreatic cancer and its early detection in the mouse. *Cancer Cell* 2003; **4:** 437–450.
35. Juin A, Spence HJ, Martin KJ, *et al*. N-WASP control of LPAR1 trafficking establishes response to self-generated LPA gradients to promote pancreatic cancer cell metastasis. *Dev Cell* 2019; **51:** 431–445.e7.
36. Hruban RH, Adsay NV, Albores–Saavedra J, *et al*. Pancreatic intraepithelial neoplasia: a new nomenclature and classification system for pancreatic duct lesions. *Am J Surg Pathol* 2001; **25:** 579–586.
37. Collins MA, Yan W, Sebolt–Leopold JS, *et al*. MAPK signaling is required for dedifferentiation of acinar cells and development of pancreatic intraepithelial neoplasia in mice. *Gastroenterology* 2014; **146:** 822–834.e7.
38. Yu X, Machesky LM. Cells assemble invadopodia-like structures and invade into matrigel in a matrix metalloprotease dependent manner in the circular invasion assay. *PLoS One* 2012; **7:** e30605.
39. Driscoll DR, Karim SA, Sano M, *et al*. mTORC2 signaling drives the development and progression of pancreatic cancer. *Cancer Res* 2016; **76:** 6911–6923.
40. Meng Z, Moroishi T, Mottier-Pavie V, *et al*. MAP4K family kinases act in parallel to MST1/2 to activate LATS1/2 in the hippo pathway. *Nat Commun* 2015; **6:** 8357.
41. Kim JW, Berrios C, Kim M, *et al*. STRIPAK directs PP2A activity toward MAP4K4 to promote oncogenic transformation of human cells. *Elife* 2020; **9:** e53003.
42. Huang H, Tang Q, Chu H, *et al*. MAP4K4 deletion inhibits proliferation and activation of CD4(+) T cell and promotes T regulatory cell generation in vitro. *Cell Immunol* 2014; **289:** 15–20.
43. Wang M, Amano SU, Roth Flach RJ, *et al*. Identification of Map4k4 as a novel suppressor of skeletal muscle differentiation. *Mol Cell Biol* 2013; **33:** 678–687.
44. Su YC, Han J, Xu S, *et al*. NIK is a new Ste20-related kinase that binds NCK and MEKK1 and activates the SAPK/JNK cascade via a conserved regulatory domain. *EMBO J* 1997; **16:** 1279–1290.
45. Baumgartner M, Sillman AL, Blackwood EM, *et al*. The Nck-interacting kinase phosphorylates ERM proteins for formation of lamellipodium by growth factors. *Proc Natl Acad Sci U S A* 2006; **103:** 13391–13396.
46. Fehon RG, McClatchey AI, Bretscher A. Organizing the cell cortex: the role of ERM proteins. *Nat Rev Mol Cell Biol* 2010; **11:** 276–287.
47. Palacios F, Price L, Schweitzer J, *et al*. An essential role for ARF6-regulated membrane traffic in adherens junction turnover and epithelial cell migration. *EMBO J* 2001; **20:** 4973–4986.
48. Monteleon CL, Sedgwick A, Hartsell A, *et al*. Establishing epithelial glandular polarity: interlinked roles for ARF6, Rac1, and the matrix microenvironment. *Mol Biol Cell* 2012; **23:** 4495–4505.
49. Goldspink DA, Gadsby JR, Bellett G, *et al*. The microtubule end-binding protein EB2 is a central regulator of microtubule reorganisation in apico-basal epithelial differentiation. *J Cell Sci* 2013; **126:** 4000–4014.
50. Grimont A, Leach SD, Chandwani R. Uncertain beginnings: acinar and ductal cell plasticity in the development of pancreatic cancer. *Cell Mol Gastroenterol Hepatol* 2022; **13:** 369–382.
51. Anand SK, Caputo M, Xia Y, *et al*. Inhibition of MAP4K4 signaling initiates metabolic reprogramming to protect hepatocytes from lipotoxic damage. *J Lipid Res* 2022; **63:** 100238.
52. Kong B, Wu W, Cheng T, *et al*. A subset of metastatic pancreatic ductal adenocarcinomas depends quantitatively on oncogenic Kras/Mek/Erk-induced hyperactive mTOR signalling. *Gut* 2016; **65:** 647–657.
53. Zhao Y, Schoeps B, Yao D, *et al*. mTORC1 and mTORC2 converge on the Arp2/3 complex to promote $Kras^{G12D}$-induced acinar-to-ductal metaplasia and early pancreatic carcinogenesis. *Gastroenterology* 2021; **160:** 1755–1770.e17.
54. Tan X, Gao Y, Nan Y, *et al*. Cellular MicroRNA let-7a suppresses KSHV replication through targeting MAP4K4 signaling pathways. *PLoS One* 2015; **10:** e0132148.
55. Roth Flach RJ, Skoura A, Matevossian A, *et al*. Endothelial protein kinase MAP4K4 promotes vascular inflammation and atherosclerosis. *Nat Commun* 2015; **6:** 8995.
56. Seo G, Han H, Vargas RE, *et al*. MAP4K interactome reveals STRN4 as a key STRIPAK complex component in hippo pathway regulation. *Cell Rep* 2020; **32:** 107860.
57. Botros L, Pronk MCA, Juschten J, *et al*. Bosutinib prevents vascular leakage by reducing focal adhesion turnover and reinforcing junctional integrity. *J Cell Sci* 2020; **133:** jcs240077.
58. Gao X, Gao C, Liu G, *et al*. MAP4K4: an emerging therapeutic target in cancer. *Cell Biosci* 2016; **6:** 56.

59. Jovanovic D, Yan S, Baumgartner M. The molecular basis of the dichotomous functionality of MAP4K4 in proliferation and cell motility control in cancer. *Front Oncol* 2022; **12:** 1059513.
60. Tripolitsioti D, Kumar KS, Neve A, *et al*. MAP4K4 controlled integrin β1 activation and c-Met endocytosis are associated with invasive behavior of medulloblastoma cells. *Oncotarget* 2018; **9:** 23220–23236.
61. Brümmendorf TH, Cortes JE, Milojkovic D, *et al*. Bosutinib versus imatinib for newly diagnosed chronic phase chronic myeloid leukemia: final results from the BFORE trial. *Leukemia* 2022; **36:** 1825–1833.

SUPPLEMENTARY MATERIAL ONLINE

Supplementary materials and methods

Figure S1. MAP4K4 deletion does not substantially impact pancreatic function

Figure S2. A loss of MAP4K4 generates minor histological differences at tumour end point

Figure S3. Loss of MAP4K4 does not affect expression of related kinases MAP4K5 and MAP5K6

Figure S4. MAP4K4 deletion does not affect linear invadosome formation or cell proliferation in PDAC cells

Figure S5. Loss of MAP4K4 does not affect YAP, P38, and JNK pathways

Figure S6. Inhibition of MAP4K4 kinase activity induces activation of AKT and ERK signalling pathways

Table S1. Animal research reporting in vivo experiments table